Noname manuscript No.
(will be inserted by the editor)

Dynamics Reconstruction and Classification via Koopman Features

Wei Zhang · **Yao-Chi Yu** · **Jr-Shin Li**

Received: date / Accepted: date

Abstract Knowledge discovery and information extraction of large and complex datasets has attracted great attention in wide-ranging areas from statistics and biology to medicine. Tools from machine learning, data mining, and neurocomputing have been extensively explored and utilized to accomplish such compelling data analytics tasks. However, for time-series data presenting active dynamic characteristics, many of the state-of-the-art techniques may not perform well in capturing the inherited temporal structures in these data. In this paper, integrating the Koopman operator and linear dynamical systems theory with support vector machines (SVMs), we develop a novel dynamic data mining framework to construct low-dimensional linear models that approximate the nonlinear flow of high-dimensional time-series data generated by unknown nonlinear dynamical systems. This framework then immediately enables pattern recognition, e.g., classification, of complex time-series data to distinguish their dynamic behaviors by using the trajectories generated by the reduced linear systems. Moreover, we demonstrate the applicability and efficiency of this framework through the problems of time-series classification in bioinformatics and healthcare, including cognitive classification and seizure detection with fMRI and EEG data, respectively. The developed Koopman dynamic learning framework then lays a solid foundation for effective dynamic data mining and promises a mathemati-

This work was supported in part by the National Science Foundation under the awards CMMI-1763070 and ECCS-1509342 and the National Institutes of Health Grants R21EY027590 and R01GM131403.

Wei Zhang
Washington University in St. Louis
E-mail: wei.zhang@wustl.edu

Yao-Chi Yu
Washington University in St. Louis
E-mail: y.yu@wustl.edu

Jr-Shin Li
Washington University in St. Louis
E-mail: jsli@wustl.edu

cally justified method for extracting the dynamics and significant temporal structures of nonlinear dynamical systems.

Keywords Koopman operators · dynamic data mining · data-driven methods · dimensionality reduction · spectral methods · time-series classification · healthcare · bioinformatics

1 Introduction

Discovering patterns and extracting information from large and complex datasets has been a compelling research topic across disciplines from statistics to biology (de Ridder et al 2013; Jain et al 2000). In the past few decades, theoretical and computational techniques involving machine learning, computational statistics, data mining, neurocomputing, and database analysis have been extensively developed to accomplish such timely tasks of data analytics (Hallac et al 2017; Shamir et al 2010; Krishnapuram et al 2004).

Many of the proposed methods, for example, those based on pure statistical or information-theoretic approaches, e.g., Bayesian information processing, were tailored for analyzing static data or data inheriting more stationary temporal structures (Zhao et al 2016; Ahn et al 2015; Sato and Nakagawa 2015; Davis et al 2007; Wilkinson 2006). Also, classical time-series analysis and statistical learning techniques often overemphasize the statistical properties of the data, while overlooking the underlying dynamic structures inherited from the time-evolution of the data. As a result, for general tasks of data analytics and learning, such as pattern recognition, dimensionality reduction, and feature learning, involving time-series that embrace rich dynamic features, state-of-the-art methods may not perform properly to capture the temporal structures in the data, which yields unsatisfactory results.

In this paper, we aim to quantitatively extract the dynamics, specifically, the time-evolution, of dynamical systems based on their time-series data generated by experiments or simulations. The extracted dynamics are then utilized for various tasks of data analytics, such as time-series data classification and pattern recognition, which provides new insight into dynamic data mining and data-driven analysis of dynamical systems. Our approach is based on the theory of Koopman operators (Koopman 1931) and linear dynamical systems (Brockett 1970). Koopman operators, named after the French-born American mathematician Bernard Koopman, are infinite-dimensional composition operators initially used to study the spectral properties of Hamiltonian systems (Koopman 1931). Owing to their nice mathematical properties, Koopman operators have been extensively used in the field of ergodic theory to characterize the ergodicity, recurrence, and topological entropy of dynamical systems (Petersen 1983; Walters 1982). In addition, the application of Koopman operator theory for spectral analysis and model reduction of systems with attractors has also been proposed recently (Mezić 2005). In general, for a finite-dimensional nonlinear dynamical system defined on a manifold, its associated Koopman operator models the nonlinear dynamics by a linear action on an infinite-dimensional vector space. This property then immediately enables the application of linear methods, such as spectral and least squares methods, to study nonlinear systems. Such a feature of 'linear transformation' from a nonlinear and finite-dimensional to a linear and infinite-dimensional domain renders a data-driven Koopman framework for analyzing the dynamics of a nonlinear system by its time-series data, which we denote as *observations*.

In recent years, inspired by the suitability of Koopman operators for analyzing dynamical systems from their observations, a stream of research focuses has been placed on computational Koopman operator theory for the purpose of inferring system dynamics and behavior from the data-driven aspect. Prominent examples ranged from the spectral decomposition of fluid mechanical systems (Rowley et al 2009; Budišić et al 2012; Mezić 2013) and the stability analysis of power systems (Susuki et al 2011, 2016; Raak et al 2016) to the study of convectively coupled waves in the atmosphere (Giannakis et al 2015). In these works, the main idea was to numerically approximate the eigenvalues and eigenfunctions of a Koopman operator by applying spectral methods to the given time-series data, which yields a finite-dimensional approximation of the Koopman operator.

In this paper, the scope of applications of the Koopman operator theory is extended to a broader range of data mining and learning tasks involving dynamical systems. In particular, by integrating the Koopman operator and linear systems theory with support vector machines (SVMs), we develop a dynamic data mining framework to extract and quantitatively represent the dynamics of a finite-dimensional nonlinear system based on its time-series data. Specifically, this framework provides an effective approach to constructing a linear state-space model that approximately represents the nonlinear flow of the time-series on a low-dimensional space, which in turn simultaneously accomplishes dimensionality reduction of high-dimensional time-series data. We further show that this dimensionality reduction gives rise to a robust classifier for dynamic data, by the use of the temporal trajectories generated by the reduced linear system as features. Moreover, we also demonstrate the robustness and applicability of this classifier by performing various classification tasks, including cognitive classification with functional magnetic resonance imaging (fMRI) data and seizure detection with electroencephalography (EEG) data. The developed methodology with the presented case studies promises a mathematically justified and systematic data-driven method for learning the dynamics and temporal structures of nonlinear dynamical systems.

This paper is organized as follows. In the next section, we first introduce some basics of the Koopman operator theory from a dynamical systems aspect, and then illustrate a data-driven viewpoint of the Koopman framework. In Section 3, the focus is to present a dynamic learning method for extracting dynamics from time-series data. In particular, we demonstrate the idea of utilizing the extracted dynamic features to embed high-dimensional time-series data to low-dimensional spaces and to construct a linear system model representing an approximation to the nonlinear dynamics. In Sections 4 and 5, the developed methodology is apply to cognitive classification and seizure detection problems using fMRI and EEG data, respectively, where we show excellent performance in such classification tasks through the developed Koopman mining approach.

2 Koopman Operators for Nonlinear Dynamical Systems

In this section, we will first briefly review the theory of Koopman operators and its connection to the study of nonlinear dynamical systems, where we also define the mathematical notations used throughout this paper. We will then leverage the dependence of the Koopman operator on the system dynamics to construct a reduced linear dynamic model including state and output variables that approximately describes the time-evolution of a nonlinear dynamical system on its state and observation spaces based on the available time-series data of this system.

2.1 Basics of the Koopman Operator

Consider a continuous-time dynamical system evolving on a manifold M described by the nonlinear differential equation

$$\frac{dx(t)}{dt} = F(x(t)), \tag{1}$$

where $x(t) \in M$ denotes the state and $F : M \to \mathbb{R}^n$ is a vector field on M. Let $\Phi : \mathbb{R} \times M \to M$ denote the flow of the system in (1), then $\Phi(t, x_0) \in M$ is the point that $x_0 \in M$ is steered to by the system in time t, and $\Phi_t \doteq \Phi(t, \cdot) : M \to M$ is a bijective function on M for every $t \in \mathbb{R}$. For a fixed time $t \in \mathbb{R}$, the Koopman operator $U : L^2(M) \to L^2(M)$ associated with the system in (1) is defined by $f \mapsto f \circ \Phi_t$, where $L^2(M) = \left\{ f : M \to \mathbb{R}^n \,\middle|\, \int_M |f|^2 dx < \infty \right\}$ denotes the space of square-integrable functions on M. More specifically, for a fixed function $f \in L^2(M)$ and a point $p \in M$, the action of the Koopman operator on f evaluated at p is given by $(Uf)(p) = f(\Phi_t(p))$. One can easily show that U is a linear operator, due to the linearity of the composition operation, on the function space $L^2(M)$. A schematic representation of the Koopman operator is illustrated in Figure 1.

Recall that the volume of M can be defined by the integral of the constant function 1 over M, i.e., $\mathrm{Vol}(M) = \int_M dx$, and M has finite volume if $\mathrm{Vol}(M) < \infty$. If the flow Φ_t is measure-preserving, i.e., for any finite measure subset S of M, it satisfies $\mathrm{Vol}(S) = \mathrm{Vol}(\Phi_t^{-1}(S))$, then the Koopman operator U associated with Φ_t is unitary (Koopman 1931; Petersen 1983; Walters 1982). Hence, by the spectral theorem (Douglas 1998), it can be decomposed by

$$U = \sum_{k=1}^{\infty} \lambda_k P_k + \int_{\mathbb{S}^1} \lambda \, dP(\lambda) = U_p + U_c, \tag{2}$$

where $\mathbb{S}^1 = \{z \in \mathbb{C} : |z| = 1\}$ is the unit circle, and $\lambda_k \in \mathbb{S}^1$ are the eigenvalues of U for $k = 1, 2, \ldots$, i.e., there exist $\varphi_k \in L^2(M)$ such that $U\varphi_k = \lambda_k \varphi_k$, P_k is the projection onto the space spanned by φ_k, and $P(\lambda)$ is a continuous resolution of the identity, i.e., for any $f \in L^2(M)$, there exists a Borel measure μ_f such that $\mu_f(\{p\}) = 0$ for any $p \in M$ and $\|U_c f\|^2 = \int_{\mathbb{S}^1} \lambda^2 d\mu_f(\lambda)$.

The idea of treating nonlinear systems with linear Koopman expansions can be illuminated by the following simple example. Consider a finite-dimensional oscillatory

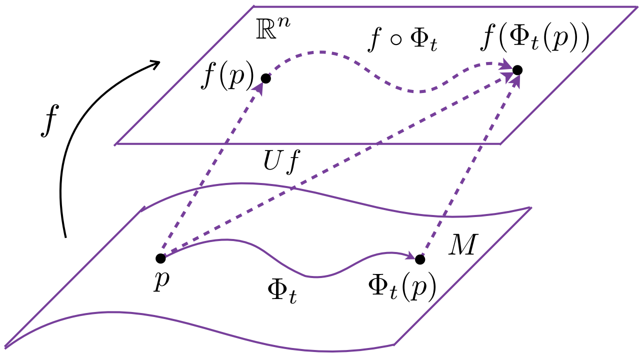

Fig. 1 A schematic representation of the Koopman operator.

system on the unit circle $\mathbb{S}^1$ with constant speed ω. The flow of this periodic system is given by $\Phi_t(e^{2\pi i\theta}) = e^{2\pi i(\theta+\omega t)}$, and hence the Koopman operator associated with this system is defined by $Uf(e^{2\pi i\theta}) = f(e^{2\pi i(\theta+\omega t)})$ for any $f \in L^2(\mathbb{S}^1)$. Because the speed is constant, Φ_t is measure-preserving, and thus U admits a spectral decomposition as in (2). One can further see that the Fourier bases $\varphi_k = e^{2\pi ik\theta}$, $k = 0, \pm 1, \ldots$, are the eigenfunctions of U since $U\varphi_k = \lambda_k \varphi_k$, where $\lambda_k = e^{2\pi ik\omega t}$ are the corresponding eigenvalues of φ_k. Together with the property that $\mathrm{span}\{\varphi_k : k = 0, \pm 1, \ldots\} = L^2(\mathbb{S}^1)$, we have for any $f \in L^2(M)$,

$$Uf = \sum_{k=-\infty}^{\infty} e^{2\pi ik\omega t}\langle f, e^{2\pi ik\theta}\rangle e^{2\pi ik\theta},$$

where $\langle f, e^{2\pi ik\theta}\rangle = \int_0^1 f(e^{2\pi i\theta})e^{2\pi ik\theta}d\theta$ is the k^{th} Fourier coefficient of f.

2.2 A Data-Driven Viewpoint of the Koopman Framework

The properties of the Koopman operator render a natural way to formulate a data-driven architecture for dynamical systems. In this context, for the dynamical system as in (1), we interpret the data (in the form of time series), denoted by y, as knowledge or realizations of the state variable x in the state space M. Then, data are functions of the state, e.g., $y = f(p)$ for $p = x(\tau) \in M$ at time τ and $y \in \mathbb{R}^n$ (see Figure 1), and we call these functions *observables* of the system. In this setting, given the time series data generated by experiments or simulations, the Koopman framework provides a precise description of the relationship between the evolution of the observables (e.g., $f(p) \mapsto f(\Phi_t(p))$) and the evolution of the state variables (e.g., $p = x(\tau) \mapsto \Phi_t(x(\tau)) = \Phi_t(p)$). More mathematically speaking, the Koopman operator is a lifting of the dynamics from the state space M to the space of observables $L^2(M)$. This lifting provides a linear rule of the evolution assigned by a Koopman operator on the space of observables $L^2(M)$, which is though infinite dimensional (Rowley et al 2009). One can further observe that the Koopman operator induces a time-series on $\mathbb{R}^n$, given by $\{f(p), (Uf)(p), \ldots, (U^k f)(p), \ldots\}$, which is exactly the 'sampled flow' of the observations of the dynamical system starting from p. This feature enables the extraction of the dynamics of a system as in (1) from its measurement data by the Koopman operator. Notice that, in practice, it is usually the case that only finitely many observations within a finite time window are available. Therefore, it suffices to require the observable f to be square-integrable on the compact subset of M whose image under f contains all of the data points for the application of Koopman operator theory from the data-driven aspect.

3 Dynamics Reconstruction from Observations

In this section, we will leverage the Koopman operator theory to extract dynamics of dynamical systems based on their measurement or simulation data. Our development is based on the utilization of spectral methods to construct reduced linear systems through the notion of orthogonal projections. The temporal trajectories of these constructed systems are viewed as embeddings of the high-dimensional time-series data to a low-dimensional space, which can then be used as features for classification tasks. In addition, we establish a preconditioning scheme by introducing an appropriate inner product on the data space so that these embeddings preserve the distance between the data points.

3.1 Matrix Representation of Data Propagation

A compelling goal for data-driven analysis of dynamical systems is to extract the dynamics of a given system from its time-series data. A meaningful way to achieve this is through the construction of a matrix representation that approximately describes the propagation of the data, e.g., $\{y_0,\dots,y_m\}$, on the observation space, typically a finite-dimensional Euclidean space, e.g., $\mathbb{R}^n$. Spectral methods (Canuta et al 2006) are powerful tools that can be employed to systematically construct such a propagation matrix. Specifically, the construction is based on first forming an order-m Krylov subspace $\mathscr{K}_y$ defined by $\mathscr{K}_y = \mathrm{span}\{y_0,\dots,y_{m-1}\}$, which is a vector space spanned by the first m data vectors, and then project the remaining data vector y_m onto $\mathscr{K}_y$. The latter step is formulated as a least squares problem, where $m \le n$, given by

$$\min_{c\in\mathbb{R}^m} \|Kc - y_m\|, \tag{3}$$

where $K = [y_0 \mid y_1 \mid \cdots \mid y_{m-1}] \in \mathbb{R}^{n\times m}$ is the matrix whose column vectors span $\mathscr{K}_y$, and $\|\cdot\| : \mathbb{R}^n \to \mathbb{R}$ is a norm on $\mathbb{R}^n$. One typical choice of $\|\cdot\|$ is the Euclidean norm, i.e., $\|x\|^2 = x'x$ for any $x \in \mathbb{R}^n$. It is well-known that $c = (K'K)^{-1}K'y_m = [c_0,\dots,c_{m-1}]' \in \mathbb{R}^m$, where '$'$' denotes the transpose operation. Using this minimizing vector, we can construct a companion matrix

$$C = \begin{bmatrix} 0 & \cdots & 0 & c_0 \\ 1 & \cdots & 0 & c_1 \\ \vdots & \ddots & \vdots & \vdots \\ 0 & \cdots & 1 & c_{m-1} \end{bmatrix} \in \mathbb{R}^{m\times m} \tag{4}$$

that approximates the flow of the given time-series data under the basis $\{y_0,\ldots,y_{m-1}\}$. This is shown by the following equation,

$$[y_1 \mid y_2 \mid \cdots \mid y_m] = [y_0 \mid y_1 \mid \cdots \mid y_{m-1}] \begin{bmatrix} 0 & \cdots & 0 & c_0 \\ 1 & \cdots & 0 & c_1 \\ \vdots & \ddots & \vdots & \vdots \\ 0 & \cdots & 1 & c_{m-1} \end{bmatrix} + r, \tag{5}$$

where r is an $n\times m$ matrix with the last column being the vector of the projection error $Kc-y_m$, and the other columns being zero vectors. In particular, the equation in (5) reveals that the matrix C advances the time-series data by one snapshot, and hence represents the flow of the data. This method is called the Arnoldi-type algorithm (Rowley et al 2009; Susuki et al 2016), and is suitable for those datasets with the spatial dimension n much higher than the temporal dimension m.

In the case in which $m > n$, namely, the number of data snapshots is greater than the dimension of each data vector, the method of vector Prony analysis can be applied (Susuki et al 2016). In this method, the Krylov subspace is constructed by $\mathscr{K}_Y = \mathrm{span}\{Y_0,\ldots,Y_{s-1}\}$, where

$$Y_k = \begin{bmatrix} y_k \\ \vdots \\ y_{k+l-1} \end{bmatrix} \in \mathbb{R}^{nl}$$

with $y_k \in \mathbb{R}^n$, $nl \geq s$, $s+l-1 = m$, and $k = 0,\ldots,s$, and the optimization problem in (3) becomes

$$\min_{c\in\mathbb{R}^s} \|Hc - Y_s\|, \tag{6}$$

where $H = [Y_0 \mid Y_1 \mid \cdots \mid Y_{s-1}] \in \mathbb{R}^{nl\times s}$ is the Hankel matrix generated by the data. Similar to the case of $m \leq n$, the companion matrix C constructed by the solution $c \in \mathbb{R}^s$ of the least squares problem in (6) also represents the dynamics of the given time-series data $y_0,\ldots,y_m \in \mathbb{R}^n$ under the basis of $\mathscr{K}_Y$.

As shown in (5), the vector c obtained by spectral methods characterizes the dynamics of the time-series data, and the companion matrix C represents the propagation of data (an exact representation from y_0 to y_{m-1} and an approximation from y_{m-1} to y_m) under the basis of $\mathscr{K}_y$ or $\mathscr{K}_Y$.

3.2 Dynamic Data Embedding and System Reconstruction

In the previous section, we introduced a systematic method to extract the dynamics of time-series data and represented the dynamics by a vector $c \in \mathbb{R}^m$, which we refer to as the dynamic feature. In this section, we will take advantage of this dynamic feature c and the companion matrix C obtained by spectral methods based on the available data to construct a low-dimensional linear model that represents an approximation to the underlying dynamical system as in (1).

3.2.1 Linear Model Construction

To begin with, suppose we are given the time-series data $y_0,\ldots,y_m$ on $\mathbb{R}^n$ generated by measurement or simulation of a system in the form of (1) through the process f (see Figure 1). Let U denote the Koopman operator associated with this system, and $x_k \in \mathbb{R}^m$ denote the state of the system at the k^{th} snapshot, then we have for $k = 0,\ldots,m$,

$$y_k = f(x_k) = (Uf)(x_{k-1}) = (U^k f)(x_0). \tag{7}$$

Consider a linear observable of the form $f(x) = Kx$, where $K = [y_0 \mid y_1 \mid \cdots \mid y_{m-1}] \in \mathbb{R}^{n\times m}$ and the set $\{y_0,\ldots,y_{m-1}\}$ forms a basis of the Krylov subspace $\mathscr{K}_y$, then from (7) we have

$$y_{k+1} = f(x_{k+1}) = (Uf)(x_k) = UKx_k. \tag{8}$$

Because $K = [f(x_0) \mid f(x_1) \mid \cdots \mid f(x_{m-1})]$, in which $f(x_k) = y_k$ for $k = 0,\ldots,m-1$, we have $UK = [Uf(x_0) \mid Uf(x_1) \mid \cdots \mid Uf(x_{m-1})] = [y_1 \mid y_2 \mid \cdots \mid y_m]$ by (7). Combining this observation with (5) and (8), we arrive

$$y_{k+1} = UKx_k = (KC + r)x_k.$$

On the other hand, we also have, by the definition of the observable f,

$$y_{k+1} = f(x_{k+1}) = Kx_{k+1}.$$

These two representations of the data point y_{k+1}lead to a reduced linear system defined on $\mathbb{R}^m$ ($m \ll n$),

$$\begin{aligned} x_{k+1} &= Cx_k, \quad x_0 = e_1, \\ z_k &= Kx_k, \end{aligned} \tag{9}$$

where $e_1 = (1,0,\ldots,0)' \in \mathbb{R}^m$, z_k denotes the output of the system on $\mathscr{K}_y$, and the projection error r is neglected. The state and output of this linear system satisfy $x_k = e_{k+1}$, $z_k = y_k$ for $k = 0,\ldots,m-1$, and $x_m = c$, $z_m = Kc$ for $k = m$, where z_m is the projection of y_m on $\mathscr{K}_y$ (see Figure 2). This reveals that the output z_k, $k = 0,\ldots,m$, describes the evolution of the time-series data y_k on $\mathscr{K}_y$, and hence the state trajectory x_k characterizes the dynamics of the time-series data on $\mathbb{R}^m$.

Similarly, if we use the vector Prony analysis method described in Section 3.1, the system in (9) will be replaced by

$$x_{k+1} = Cx_k, \quad x_0 = e_1, \tag{10}$$

$$z_k = Hx_k, \tag{11}$$

which defines a linear system on $\mathbb{R}^s$ that models the dynamics of the time-series $Y_0,\ldots,Y_s$, constituted by $y_0,\ldots,y_m$, on the Krylov space $\mathscr{K}_Y = \text{span}\{Y_0,\ldots,Y_{s-1}\}$, and where H is the Hankel matrix as defined in (6).

Note that, from the control-theoretic point of view, the system in (9) is in an observability canonical form (Brockett 1970). Therefore, this model is structurally convenient for control analysis and design, such as pole assignment and feedback control design.

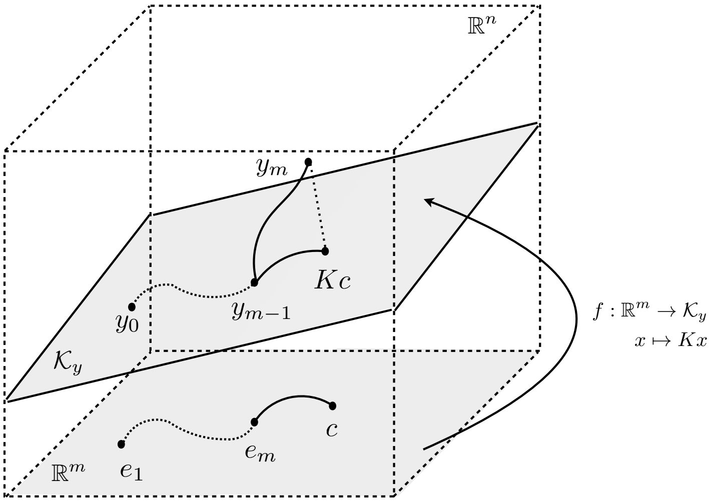

Fig. 2 A schematic representation of the dynamics of the reduced linear system. The state and the output of the system flow from e_1 to c on $\mathbb{R}^m$ and y_0 to Kc on $\mathscr{K}_y$, respectively, where $\mathscr{K}_y = \text{span}\{y_0, \dots, y_{m-1}\}$, $K = [y_0 \mid \cdots \mid y_{m-1}]$, and c is the least-squares solution of $Kc = y_m$, or equivalently, Kc is the point orthogonally projected from y_m onto $\mathscr{K}_y$.

3.2.2 Preconditioning by Orthogonality of Time-Series Data

In Section 2.1, the spectral decomposition of the Koopman operator is applied under the condition that U is unitary. One of the most important consequences of the unitarity is that U is a linear isometry, i.e., U preserves the norm of every observable, i.e., $\|Uf\| = \|f\|$ for any $f \in L^2(M)$. In the following, we will introduce a scheme for preconditioning the data so that the recovered Koopman operator preserves the norm of the data points, and hence also preserves the norm of the observable generating the data. In the case of $n > m$, such a norm can be induced by an inner product g on $\mathbb{R}^n$ satisfying $\|y_i\|_g^2 = y_i' g y_i = 1$ for $i = 0, \dots, m$, where $y_0, \dots, y_m$ are the given time-series. Then, the optimization problem in (3) under this norm will be considered, which is given by

$$\min_{c \in \mathbb{R}^m} \|Kc - y_m\|_g. \tag{12}$$

In particular, a preferred inner product g is the one that transforms the basis vectors $y_0, \dots, y_{m-1}$ of $\mathscr{K}_y$ to an orthonormal set. In this case, because the output function $f(x) = Kx$ maps the orthonormal basis $\{e_1, \dots, e_m\}$ for $\mathbb{R}^m$ onto the orthonormal basis $\{y_0, \dots, y_{m-1}\}$ for $\mathscr{K}_y$, f is a linear isometry under the inner product g, i.e., $\|f(x)\|_g = \|x\|$. Consequently, the embedding of the time-series data from $\mathbb{R}^n$ to $\mathbb{R}^m$, induced by the system in (9), preserves the g-distance, for example, $\|y_{i+1} - y_i\|_g = \|f(e_i) - f(e_{i-1})\|_g = \|e_i - e_{i-1}\| = \sqrt{2}$. Similarly, in the case of $n < m$, the inner product g will be introduced on $\mathbb{R}^{nl}$ to orthonormalize $Y_0, \dots, Y_s$ which are constituted by $y_0, \dots, y_m$. This distance-persevering property further implies that the embedding maintains the local structure of the time-series data by implementing the preconditioning scheme.

3.3 Koopman Dimensionality Reduction and Embedding

The reduced linear models, characterized by the pairs (C,K) and (C,H) in (9) and (10), respectively, derived from the Koopman framework are dimensionality reductions, where (C,K) and (C,H) serve as the embeddings of the high-dimensional time-series data $y_k \in \mathbb{R}^n$, $k = 0,\ldots,m$, onto the low-dimensional space, $\mathbb{R}^m$ or $\mathbb{R}^s$ (see the case studies in Sections 4 and 5). Moreover, the construction of such 'dynamics-preserving' embeddings only involves solving least-squares problems with minor computational efforts. Therefore, the established Koopman framework offers a novel, efficient, and systematic dynamic data mining approach to extracting dynamic features and reducing dimensionality of complex time-series data. Note that our approach is based on the utilization of the Koopman operator theory to linearly transform a finite-dimensional nonlinear system to an infinite-dimensional linear system. Theoretically, if infinitely many snapshots of an unknown system are available, the dynamics reconstruction can be achieved arbitrarily well. Practically, the proposed approach will perform better if more observation samples are available and the dynamics of the underlying unknown system is more time-invariant.

In following sections, this Koopman framework will be integrated with machine learning techniques to analyze dynamics of brain systems. Specifically, temporal patterns of brain systems are decoded into dynamic features and embedded trajectories. These quantities are then good candidates of learning features for some classifier to distinguish different brain activities. Figure 3 illustrates the application of the Koopman framework to brain systems. Moreover, the developed methodology will be validated by using two time-series datasets of different modalities: an fMRI visual cognition dataset for cognitive classification and an EEG dataset for seizure detection. In particular, we will show that leaning features extracted by the Koopman method will lead to excellent performance of classifiers, which in turn extends the scope of the applications of the Koopman operator theory to the fields of bioinformatics and healthcare.

4 Cognitive Classification

Functional magnetic resonance imaging (fMRI) is a neuroimaging technique used to measure brain activities by detecting changes associated with blood flow (Huettel et al 2008). In neuroscience, fMRI is widely used to study responses of the brain to external stimuli (Coutanche et al 2011; Smith 2004). Nowadays, multivoxel pattern analysis (MVPA) is a popular data-driven method to identify brain response patterns through fMRI images, where voxels of images are taken as feature vectors to train a high-dimensional classification model (Ma et al 2016; Chou et al 2014; Martino et al 2008). In our analysis, fMRI data is treated as observations of some unknown dynamical system. The Koopman framework is then adopted to linearly approximate

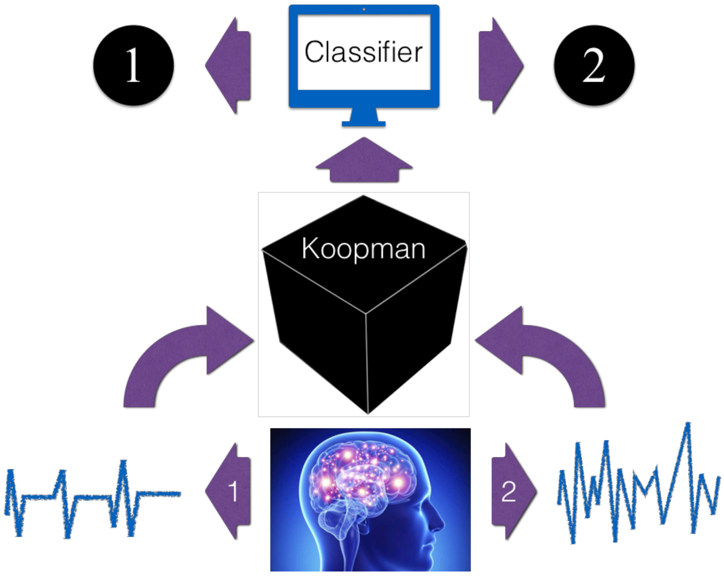

Fig. 3 An illustration of the application of Koopman framework to brain systems. The Koopman operator theory provides a tool to extract dynamics-related quantities from time-series data, e.g., dynamic features and embedded trajectories. These quantities then serve as learning features for some classifier to distinguish data representing different brain dynamics. For example, two different kinds of brain activities, labeled by 1 and 2, are documented in some time-series data. The Koopman framework provides a systematic method to determine the label of the given time-series, i.e., the brain activity that the time-series records.

the brain activities captured by the fMRI data, as well as embed the high-dimensional fMRI data onto a low-dimensional space to efficiently facilitate cognitive classification.

4.1 Dataset Description

In this work, we use the block-design fMRI dataset experimented by James V. Haxby's research group in 2001 (Haxby et al 2001). The purpose of this experiment was to study the face and object representation in human ventral temporal cortex. The experiment consists of 6 subjects, and each subject was asked to run the experiment 12 times. In each run of the experiment, eight greyscale images were shown to one subject, with each image displaying for 500ms. At the same time, full-brain fMRI was recorded with a volume repetition time of 2.5s, and each stimulus block was covered by 9 discrete-time data points. The data for the ninth experiment of subject 5 was corrupted, so we will not consider this subject in the following analysis. As a result, we have in total 864 (12 runs $\times$ 8 images $\times$ 9 points) fMRI datapoints for each of the 5 considered subjects. Every datapoint is a vector containing voxels that document the brain activity in the corresponding subject's ventral temporal cortex. Sizes of the 5 subjects' ventral temporal cortex, i.e., dimensions of the data vectors for the

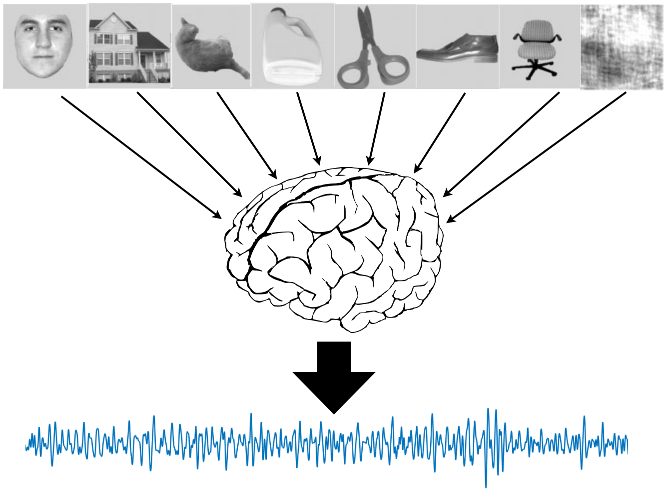

Fig. 4 An illustration of the block-design fMRI experiment. In the experiment, full-brain fMRI was recorded, while eight greyscale images were shown to each subject.

5 subjects, are 577, 464, 307, 675, and 348, respectively. The experiment setting is illustrated in Figure 4.

4.2 Extraction of Brain Dynamics

In the described experiment, e.g., for the first subject, 577-dimensional time-series data containing 9 snapshots were recorded for each run. From the dynamical systems point of view, the flow of these 9-snapshot fMRI data reflects the subjects' brain activities in response to the images shown to him or her in the experiment. Consequently, classifying the fMRI image data is a meaningful way to distinguish the subject's cognitive responses to different external stimuli (image-viewing). To this end, we utilize the technique of dynamics extraction developed in Section 3.1 to capture the subjects' brain activities. Specifically, the Arnoldi-type algorithm (Susuki et al 2016; Mezić 2013) is applied to construct an 8-dimensional Krylov subspace $\mathscr{K}_y = \text{span}\{y_0, \ldots, y_7\}$. By projecting the last data vector y_8 onto $\mathscr{K}_y$, the dynamics of every sequence of the 577-dimensional time-series data is documented into an 8-dimensional vector c (dynamic feature). Therefore, we obtain 96 (12 runs $\times$ 8 images) such 8-dimensional dynamic features in total for each of the 5 considered subjects, and every dynamic feature is a quantification of one subject's brain activity responding to one image.

4.3 Classification by Embedded Trajectories

According to the discussion in Section 3.2, the extracted dynamic features, represented by vectors in $\mathbb{R}^8$, can be used to construct linear systems in their observability

Table 1 The accuracy of cognitive classification by using the 20-snapshot trajectories.

Subject No.	Euclidean projection	Non-Euclidean projection
1	0.96	0.97
2	0.91	0.96
3	0.89	0.94
4	0.83	0.85
6	0.80	0.98
Average	0.88	0.94

canonical forms as in (9), and the state trajectories of these reduced systems are the embeddings of the high-dimensional fMRI data onto the low-dimensional space $\mathbb{R}^8$. To distinguish the brain dynamics in response to different images, SVMs are utilized to classify these low-dimensional trajectories. Specifically, for each of the constructed linear systems, we generate a 20-snapshot trajectory as a feature for the SVM classifier, in which we use the l^2-norm, defined by

$$\|x - x'\|_{l^2} = \sqrt{\sum_{i=0}^{19} \|x_i - x'_i\|^2},$$

to measure the distance between different trajectories x and x', where x_i and x'_i are in $\mathbb{R}^8$ denoting the i^{th} snapshot of x and x', respectively, and $\|\cdot\|$ is a norm on $\mathbb{R}^8$. For each subject, 95 out of the 96 trajectories are used to train a learning model, and the remaining one trajectory is used to test the accuracy of the model. In addition, as we proposed in Section 3.2.2, a non-Euclidean inner product can be introduced on the data space to orthonormalize the 8 data points spanning $\mathscr{K}_y$. Notice that for the same subject and image, the dynamic features obtained by non-Euclidean projections are different from those obtained by Euclidean projections. Consequently, the resulting linear systems and their trajectories are also different, although they represent the same brain activity, in the view of different bases or coordinate systems. In our study, we also use those trajectories obtained by non-Euclidean projections to classify the brain activities. Table 1 shows the classification accuracy by using the 20-snapshot trajectories as features obtained from both of the Euclidean and non-Euclidean projections.

4.4 Classification by Dynamic Features

We also employ SVMs to directly classify those 8-dimensional dynamic features extracted from the fMRI time-series data. Similar to the trajectory classification described in the previous section, for each subject, one vector from the 96 dynamic features is picked randomly as the test data, and the remaining 95 of them are used to train a model. Table 2 shows the accuracy of the classification based on the 8-dimensional dynamic features.

Table 2 The accuracy of cognitive classification by using the 8-dimensional dynamic features.

Subject No.	Euclidean projection	Non-Euclidean projection
1	0.83	0.89
2	0.87	0.93
3	0.47	0.78
4	0.64	0.69
6	0.77	0.99
Average	0.72	0.86

4.5 Discussion of the Cognition Classification Results

Comparing Table 1 with Table 2, classifying the 20-snapshot trajectories of the reduced linear systems results in higher accuracy than classifying the 8-dimensional dynamic features. Especially, in the case of Euclidean projections, the classification accuracy of subject 3 is greatly improved by using the trajectories instead of the dynamic features, where the accuracy increases from 0.471 to 0.888. This observation highlights that the embedded trajectories more accurately represent the dynamics of the time-series data than the dynamic features do.

A great advantage of using the reduced linear systems in classification problems is the ability to generate longer trajectories, although the original time-series data is of limited temporal dimension. Taking the fMRI dataset as an example, we generated a trajectory of length 20, while the temporal dimension of the fMRI data is only 9. From the machine learning aspect, this means that we are able to obtain more features for the classifiers to learn models for distinguishing different brain activities.

Moreover, each of Tables 1 and 2 is also self-contained: the non-Euclidean orthonormal projections always lead to better classification accuracy than the Euclidean projections do, which can be explained by using the Koopman operator theory as follows. Recall the Koopman operator theory introduced in Section 2, the dynamic feature extracted from the time-series data induces a companion matrix, whose eigenvalues and eigenvectors approximate those of the Koopman operator by the spectral theorem. However, the application of the spectral theorem requires the Koopman operator to be unitary. The non-Euclidean inner product provided in Section 3.2.2 simultaneously orthogonalizes and normalizes the time-series data vectors, and this renders the distance-preserving property of the dimensionality reduction of the time-series, which is also a necessary condition to guarantee the unitarity of the approximated Koopman operator. The greater classification accuracy by using non-Euclidean projections shown in Tables 1 and 2 then validates that unitarity of Koopman operators indeed helps with distinguishing the dynamics of different systems in the form of (9).

4.6 Comparison of Feature Selection Methods for Cognitive Classification

In the previous section, we showed the promising performance of the cognitive classification by using different feature generation methods based on the Koopman framework developed in Section 3. In the widely used multi-voxel pattern analysis (MVPA)

Table 3 Comparison of cognition classification results by Koopman features and MVPA.

Subject No.	Trajectories	MI + PSR	SFS	SBS	PSO	HHPSO
1	0.97	0.88	0.39	0.80	0.92	0.95
2	0.96	0.75	0.27	0.62	0.69	0.80
3	0.94	0.85	0.33	0.82	0.85	0.87
4	0.85	0.69	0.36	0.55	0.80	0.85
6	0.98	0.88	0.45	0.73	0.82	0.84
Average	0.94	0.81	0.36	0.70	0.82	0.86

for fMRI data, the data points representing the voxels are directly used as features for classifiers. Various feature selection approaches for MVPA have been recently proposed to increase the classification accuracy. These include mutual information (MI) based method, partial least-squares regression (PSR), sequential forward feature selection (SFS), sequential backward feature selection (SBS), particle swarm optimization (PSO), and hierarchical heterogeneous particle swarm optimization (HHPSO) (Chou et al 2014; Ma et al 2016; Michel et al 2008; Mitchell et al 2008; Liu and Motoda 1998). In this section, we compare the cognitive classification results obtained by our Koopman learning technique with the results obtained by the MVPA-based methods, in which SVMs are the chosen classifiers. The classification results are shown in Table 3. Specifically, the first column shows the accuracy of classifying the 20-snapshot trajectories obtained by the non-Euclidean projections, and the second column shows the accuracy of classifying features that are simultaneously selected by the MI and PSR methods. It is evident that the Koopman learning framework outperforms the MVPA-based methods. This further indicates that interpreting brain activities from a dynamical systems perspective lays a solid foundation for understanding brain responses to external stimuli in cognitive science, and the Koopman framework provides a mathematically justified and effective data-driven approach to capturing brain activities.

Remark 1 Haxby's research on this fMRI dataset has demonstrated that each category of objects in the displayed images evokes a unique pattern of response in cortex (Haxby et al 2001). However, it could be possible that the same category of images may elicit distinct brain activities in different runs of experiments. To test this hypothesis, we analyze the dataset by removing some dynamic features from one run of experiments. Specifically, we start with completely removing 8 dynamic features from one run of experiments, then one of the remaining 88 dynamic features is randomly chosen as the test data, and the other 87 dynamic features are used to train the classifier. On the other hand, we keep all of the 88 dynamic features in the training dataset, and pick one of the removed 8 dynamic features as the test data. Table 4 shows the classification accuracy obtained by training 87 and 88 dynamic features as described above. Notice that the classifier trained by 88 dynamic features shows much worse performance than the one trained by 87 dynamics features. This suggests that each subject's brain activity responding to a picture in one run may differ from his or her brain activities responding to the same picture in other runs. This argument is also supported by the plot shown in Figure 5, where we add the 8 removed dynamic

Table 4 Classification accuracy obtained by training 87 (11 runs leaving out 1 feature selected as the test data) and 88 dynamic features. In particular, the case of training 88 dynamic features (using all selected 11 runs of data) with the test feature picked from the removed run shows much worse performance than the case of training 87 dynamic features with the test feature picked from the selected 11 runs. This verifies the hypothesis that the same category of images may elicit distinct brain activities in different runs of experiments.

	Removed run No.	Subject 1	Subject 2	Subject 3	Subject 4	Subject 6
Training 87 dynamic features	1	0.84	0.87	0.40	0.60	0.57
	2	0.78	0.75	0.48	0.57	0.62
	3	0.84	0.80	0.48	0.54	0.60
	4	0.84	0.89	0.51	0.47	0.55
	5	0.85	0.82	0.40	0.60	0.66
	6	0.86	0.83	0.36	0.66	0.62
	7	0.88	0.86	0.41	0.55	0.62
	8	0.92	0.68	0.44	0.78	0.62
	9	0.89	0.82	0.48	0.61	0.69
	10	0.71	0.89	0.49	0.46	0.64
	11	0.84	0.74	0.38	0.70	0.55
	12	0.76	0.86	0.46	0.67	0.65
Average		0.84	0.82	0.44	0.60	0.62
Training 88 dynamic features	1	0.12	0.00	0.26	0.14	0.13
	2	0.13	0.00	0.00	0.15	0.00
	3	0.10	0.12	0.00	0.26	0.13
	4	0.00	0.12	0.13	0.26	0.12
	5	0.12	0.13	0.12	0.13	0.12
	6	0.13	0.13	0.00	0.13	0.14
	7	0.14	0.12	0.26	0.00	0.13
	8	0.13	0.11	0.00	0.00	0.00
	9	0.14	0.13	0.00	0.11	0.10
	10	0.26	0.13	0.00	0.12	0.14
	11	0.12	0.11	0.00	0.00	0.14
	12	0.24	0.13	0.00	0.00	0.14
Average		0.13	0.10	0.06	0.11	0.11

features from one complete run one-by-one into the training dataset and randomly select one of the remaining dynamic features as the test data for the leave-one-off cross validation. In particular, the removed run is selected sequentially, and the result is obtained by averaging the accuracy over all 12 cases, where each case corresponds to the removal of one of the 12 runs. Notice that when 7 dynamic features from the removed run are added into the training dataset, the classification result coincides with what we have shown in Table 2.

5 Seizure Detection

Electroencephalography (EEG), similar to the function of fMRI, is also a technique to record brain activities. To be more precisely, it measures voltage fluctuations resulting from ionic current within the neurons of the brain (Schomer and da Silva 2010). In clinical contexts, EEG serves as an important tool to diagnose diseases caused

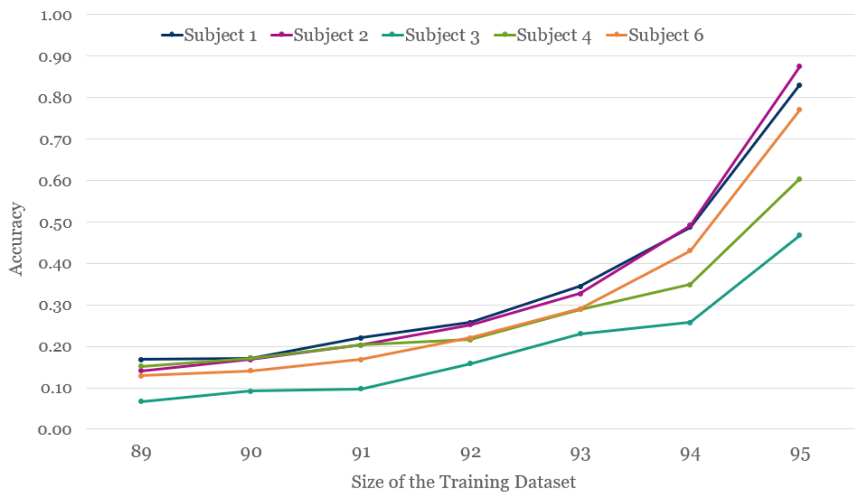

Fig. 5 Classification accuracy with respect to the size of training dataset for all of the 5 considered subjects.

by neurological disorders, for example, epileptic seizures. Conventionally, monitoring brain activities by EEG relies on the visual inspection of the recorded signals by professional neurophysiologists. Moreover, different patients may have different seizure symptoms so that visual detection is not always efficient and accurate enough for instant treatment. Therefore, more and more data mining and statistical learning methods are proposed to accurately and timely analyze EEG signals for seizure detection. One major challenge to analyzing EEG signals is their high nonlinearity and low signal-to-noise ratio (SNR), since EEG signals are not robust to external disturbance. In this situation, statistical properties of EEG signals, such as autocorrelation, variance, power spectrum, and so on, are preferred as features for some classifiers to recognize seizure and non-seizure states, after some signal enhancement approaches such as common spatial patterns (CSP) and principal component analysis (PCA) (Khanmohammad and Chou 2016, 2018; Giannakaki et al 2014; Lehnertz et al 2017). In addition to the classification based on statistical features, dynamic mode decomposition (DMD) was recently proposed to extract spatial-temporal patterns of intracranial electroencephalography (iEEG) data for clustering sleep spindle networks, where such patterns are represented in terms of eigenvalues and eigenvectors of augmented data matrices (Brunton et al 2016). In our approach proposed in this section, instead of performing statistical or spectral analysis, piecewise linear approximations of EEG dynamics are constructed through the developed Koopman framework, which gives rise to a robust classifier to distinguish the seizure and non-seizure dynamics.

5.1 Dataset Description

In this section, we validate our Koopman framework by implementing it to a public pediatric seizure dataset collected at Children's Hospital Boston (Goldberger et al

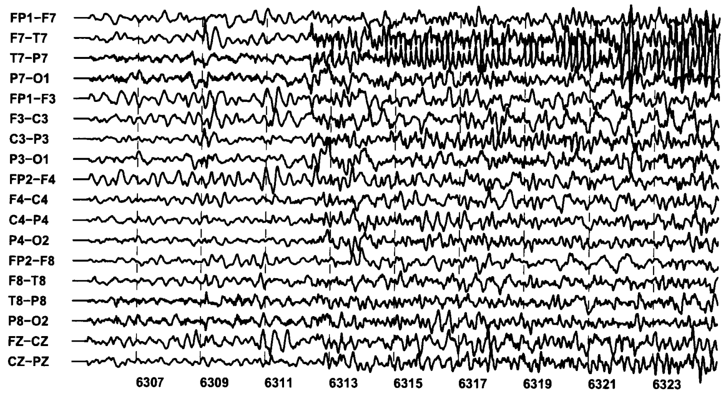

Fig. 6 EEG signals containing abnormal rhythmic activity (Shoeb 2009). The seizure begins at the 6313^{th} second, which can be readily recognized by the EEG signals in the channels F7 - T7 and T7 - P7.

2000). This dataset is also known as CHB-MIT, and it contains scalp EEG signals for 24 patients. For each patient, EEG signals of 9 to 42 hours were recorded in multiple files. In addition, the time gaps between different files, where no signal was recorded, are mostly no more than 10 seconds. Most of the files contain 23 channels of EEG signals, and few files contain 24 or 26 channels. All of the EEG signals were sampled at 256 samples per second with 16-bit resolution, and the International 10-20 system was applied to keep track of the electrode settings. Parts of the EEG signals containing a seizure onset are shown in Figure 6.

5.2 Extraction of EEG Dynamics

The most significant difference between EEG and fMRI datasets is that EEG signals have a very high ratio of temporal to spatial dimension. In our analysis, the number of channels of the EEG recordings is interpreted as the spatial dimension of the EEG dataset, which is in the range of 23 to 26. The duration of the recordings in each file mostly lasts for one hour long. This gives the EEG signals, for example, those recorded with 23 channels, the spatial and temporal dimension of 23 and 921,600 (256 samples $\times$ 3600 seconds), respectively. Therefore, the method of vector Prony analysis introduced in Section 3.1 is preferred to extract the dynamics of the EEG signals.

In addition, since EEG signals are not robust to external disturbance, filtering serves as an important step to increase SNR before conducting any further analysis. Specifically, we use a 10th-order Butterworth bandpass filter with the cutoff frequencies 2 and 10 Hz and the sampling rate of 256 per second. The selected sub-band contains all the information required to characterize the seizure behavior: delta (0.1-3 Hz), theta (4-7 Hz), and alpha (8-12.5 Hz). Furthermore, we also precondition the EEG time-series data by downsampling it. Although this may result in the loss of information, it helps with capturing the overall trend of the dynamics. Specifically, we downsample the EEG signal to the rate of 32 per second, then concatenate 32 snapshots of the downsampled signal into one Prony vector, and hence each Prony vector contains 1-second evolution of the EEG signal. The next step is to extract dynamic features that represent the dynamics of the EEG signals by applying the method of vector Prony analysis introduced in Section 3.1. To determine the appropriate dimension of the dynamic features, we formulated an optimization problem to maximize the classification accuracy over the dimension of the Krylov subspace. The solution to this optimization problem is 4 , i.e., dynamic features generated by projecting the 5th snapshot to the space spanned by its previous 4 snapshots lead to the best classification result.

Similar to the cognitive classification presented in Section 4.2, these 4-dimensional dynamic features are used to construct reduced linear systems to approximate the dynamics of the EEG signals. However, due to the high nonlinearity of the EEG signals, linear approximation may not be accurate enough to recover the actual dynamics. In the following section, we extend the developed Koopman framework to construct a piecewise linear approximation of the EEG dynamics.

5.3 Piecewise Linear Approximation of EEG Dynamics

Let $Y_0, \ldots, Y_{rm}$ be a sequence of concatenated EEG data used for applying the method of vector Prony analysis as described in the above section, i.e., each Y_i contains one second evolution of the downsampled EEG signals, then we can generate r Krylov subspaces $\mathscr{K}_1, \ldots, \mathscr{K}_r$ of dimension m, where $\mathscr{K}_i = \mathrm{span}\{Y_{(i-1)m}, \ldots, Y_{im-1}\}$. The application of the Prony method to these r Krylov subspaces yields r dynamic features, $c_1, \ldots, c_r \in \mathbb{R}^m$. Next, we concatenate these dynamic features, i.e.,

$$c = \begin{bmatrix} c_1 \\ \vdots \\ c_r \end{bmatrix} \in \mathbb{R}^{rm},$$

to obtain an aggregated dynamic feature c. Notice that because each c_i gives rise to a linear approximation of the EEG dynamics, the aggregated dynamic feature c enables a *piecewise linear approximation* scheme of the EEG dynamics under r coordinate charts. Specifically, applying the method developed in Section 3.2 to each of the dynamic features c_i, $i = 1, \ldots, r$, yields r linear systems. Concatenating the trajectories of these r systems then gives a local embedding of the EEG data to $\mathbb{R}^m$. Alternatively, the aggregated trajectory can be equivalently generated by the following piecewise linear system,

$$\begin{aligned} x_{k+1} &= f(x_k), \quad x_0 = e_1 \\ y_k &= h(x_k) \end{aligned} \tag{13}$$

where

$$f(x_k) = \begin{cases} C_1 x_k, & \text{if } 0 \leq k \leq m-1, \\ \vdots & \vdots \\ C_i x_k, & \text{if } (i-1)m \leq k \leq im-1, \\ \vdots & \vdots \\ C_r x_k, & \text{if } k \geq rm, \end{cases}$$

$$h(x_k) = \begin{cases} H_1 x_k, & \text{if } 0 \leq k \leq m-1, \\ \vdots & \vdots \\ H_i x_k, & \text{if } (i-1)m \leq k \leq im-1, \\ \vdots & \vdots \\ H_r x_k, & \text{if } k \geq rm, \end{cases}$$

$H_i = [Y_{(i-1)m} \ \cdots \ Y_{im-1}]$, and C_i is the companion matrix induced by c_i for each $i = 1, \ldots, r$. In particular, the initial condition of the first system is the first standard basis vector e_1 of $\mathbb{R}^m$. Inductively, the initial condition of the successive system is then set to be the final state of its predecessor. Furthermore, this choice of initial conditions for each system in the concatenation also guarantees that the reduced flow, i.e., the trajectory of the concatenated system, indeed represents the dynamics of the time-series data. In the next section, we will perform seizure event detection based on the concatenated trajectories and dynamic features c.

5.4 Binary Classification for Seizure Event Detection

Seizure event detection is to identify seizures with the greatest possible accuracy. The first seizure event detector was created by J. Gotman in 1982 (Gotman 1982). An experiment of the Gotman's detector showed that the algorithm can detect 50% of the tested seizures (Saab and Gotman 2005). Following Gotmam's work, many algorithms have been proposed in recent years to increase the detection accuracy (Wilson et al 2004; Wilson 2005, 2006; Khan et al 2012; Alotaiby et al 2015). One of the most famous ones is called the Reveal algorithm, whose detection accuracy is 76% on average (Wilson et al 2004). For patient-specific detections, the accuracy of the Reveal algorithm can be improved up to 78% (Wilson 2005, 2006).

In our approach, each patient's EEG signal is divided into multiple seizure and non-seizure windows, where, for example, seizure windows are time intervals in which seizure happens. For each window, we generate one trajectory of the piecewise linear system in (13) containing 16 snapshots, and then apply a binary classifier to all of such trajectories using libsvm package in MATLAB R2017a to detect the time windows over which seizures happen. Specifically, we concatenate two 4-dimensional dynamic features for each window, i.e., $r = 2$ and $m = 4$, to construct a

Table 5 Seizure event detection accuracy by classifying concatenating trajectories.

Case No.	Euclidean projection	Non-Euclidean projection
1	0.777	0.778
5	0.853	0.853
8	0.771	0.778
10	0.835	0.843
Average	0.809	0.813

Table 6 Seizure event detection accuracy by classifying concatenating dynamic features.

Case No.	Euclidean projection	Non-Euclidean projection
1	0.752	0.748
5	0.837	0.868
8	0.760	0.777
10	0.824	0.837
Average	0.793	0.808

piecewise linear system in the form of (13). We pick the cases 1, 5, 8 and 10 as examples to show the seizure event detection results in Table 5. In addition to detecting seizure windows based on trajectories, we also conduct the same binary classification on those concatenated dynamic features, and the results are shown in Table 6. For both of these two feature section scenarios, the seizure detection accuracy is higher than the Gotman and Reveal algorithms.

Comparing Table 5 with Table 6, we notice similar classification results based on the concatenated trajectories and dynamic features, although trajectories are supposed to more accurately represent the dynamics of the EEG signals as discussed in Section 4.5. This then implies that, for time-series data with highly nonlinear dynamics like EEG signals, concatenating more dynamic features results in a better representation and thus a more accurate approximation to the actual dynamics. Moreover, classification by concatenated state trajectories still outputs slightly better accuracy because in our implementations they contain more snapshots than the data used for dynamic feature extraction.

5.5 Binary Classification for Seizure Onset Detection

In addition to seizure event detection, seizure onset detection algorithms are more extensively explored (Khanmohammad and Chou 2018, 2016; Nasehi and Pourghassem 2013; Alotaiby et al 2015; Shoeb 2009). The purpose of seizure onset detection is to recognize the start of a seizure with the shortest possible delay. Generally, the performance of a seizure onset detector is evaluated by its sensitivity (S), false alarm rate (F), and latency (L), which are defined as follows. Let N_s and N_{ns} denote the number of seizure onsets and non-seizure records, respectively, s_i be a binary variable with value 1 if the i^{th} seizure is detected and 0 otherwise, f_i be another binary variable taking value 1 if the seizure alarm is triggered for the i^{th} non-seizure record, and τ_i denote the time delay between the onset of the i^{th} seizure shown in the EEG signal and the detection recognition of this seizure, then

$$S = \frac{1}{N_s}\sum_{i=1}^{N_s} s_i, \quad F = \frac{1}{N_{ns}}\sum_{i=1}^{N_{ns}} f_i, \quad L = \frac{1}{N_s}\sum_{i=1}^{N_s} \tau_i.$$

In this section, dynamic features obtained by non-Euclidean projections are used as features for the SVM classifier to design the seizure onset detector. Specifically, features of seizure and non-seizure records are labeled by 1 and 0, respectively. In order to increase the robustness of our detector to external disturbance, the seizure alarm will be triggered if three consecutive 1 are detected. Recall that in the EEG dynamics extraction procedure, one second evolution of the EEG signal is represented by one dynamic feature. Therefore, detecting three consecutive 1 requires three seconds of ictal EEG signals, which implies that the latency of the designed seizure onset detector is $L = 3$ seconds.

In Table 7, we compare the performance of the seizure onset detectors designed by the Koopman framework and SVM classifiers with other published methods: the CSP feature extraction with KNN classifiers (Khanmohammad and Chou 2016), statistical and morphological feature extraction with ADCD classifiers (Khanmohammad and Chou 2018), features extracted from different frequency bands with IPSONN classifiers (Nasehi and Pourghassem 2013), and features extracted from different frequency bands with SVM classifers (Alotaiby et al 2015). In particular, the detector designed by the Koopman framework shows very high sensitivity and relatively low latency. However, the tradeoff of the low latency is the relatively high false alarm rate. Figure 7 plots the false alarm rate versus the latency, where the false alarm rate is dramatically decreased by increasing the latency. For all of the considered four cases, the false alarm rates drop more than 400% by only doubling the latency, and particularly, the false alarm rate of case 5 drops 1300%.

Remark 2 In cognitive and behavioral neuroscience, fMRI and EEG are techniques used to measure and record brain activities in some specific neural substrates. Because brain activities vary with time, the inherent temporal structures and evolution are important for the understanding and characterization of brain functions, e.g., cognition, or brain disorders, e.g., seizures. In the proposed dynamic data mining framework, brain activities are treated as the output of a dynamical system, and the system representing brain dynamics in the neural substrates recorded with fMRI or EEG data is effectively and precisely reconstructed. The two case studies in cognitive classification and seizure detection show a great promise of using the dynamical systems idea and the Koopman mining approach to time-series analysis in basic and computational neuroscience.

6 Conclusion

In this paper, we develop a novel dynamic data mining framework that provides a systematic and effective approach to extracting dynamics of nonlinear systems using

Table 7 Comparison of seizure detection methods using CHB-MIT dataset.

Feature Extraction	Classifier	Case No.	Sensitivity (%)	False alarm rate (/h)	Latency (s)
CSP	KNN	1	100%	2.22/h	0.94
		5	75%	1.19/h	0.94
		8	100%	0.45/h	1.34
		10	100%	1.83/h	0.94
		Average	93.75%	1.42/h	1.04
Statistical + Morphological	ADCD	1	100%	0.17/h	2.5
		5	80%	0.2/h	20
		8	100%	0.15/h	2.5
		10	100%	0.03/h	7.5
		Average	95%	0.14/h	8.13
Energy in different frequency bands	IPSONN	1	100%	-	-
		5	100%	-	-
		8	100%	-	-
		10	100%	-	-
		Average	100%	0.13/h	3
Energy in different frequency bands	SVM	1	90%	-	-
		5	100%	-	-
		8	100%	-	-
		10	-	-	-
		Average	96%	-	-
Koopman	SVM	1	100%	4.87/h	3
		5	100%	0.91/h	3
		8	100%	4.77/h	3
		10	100%	2.42/h	3
		Average	100%	3.24/h	3

their time-series data. Our method integrates the Koopman operator and linear systems theory to construct a linear model that approximately represents the dynamics of a nonlinear system on a linear space of reduced dimension based on the available time-series data. The established reduced linear model is also a dimensionality reduction of high-dimensional time-series data to a low-dimensional linear space. In particular, we use the temporal trajectories generated by this low dimensional linear system as features in machine learning to classify time-series data in terms of the 'distinction' of system dynamics. The proposed data-driven method for learning dynamics of nonlinear systems is highly efficient, because the essential step is to solve least-squares problems induced by the spectral method, which is of low computational complexity and effort. Furthermore, we demonstrate the applicability and robustness of the developed methodology by studying pattern recognition problems in bioinformatics and healthcare, including cognitive classification and seizure detection using public fMRI and EEG datasets, respectively. In particular, by comparing with the state-of-the-art algorithms, we show the promise of our approach to reporting highly accurate and convincing classification results. Moreover, the developed operator-theoretic data-driven method not only illuminates new insight into devising novel mining and learning techniques for extracting dynamics of nonlinear systems,

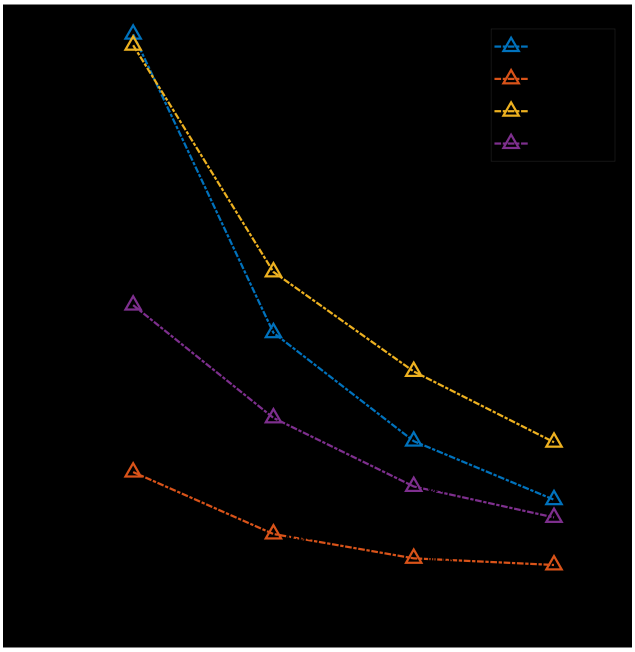

Fig. 7 The plot of the false alarm rate versus the latency for Cases 1, 5, 8, and 10, in which the false alarm rate is dramatically decreased with the increase of the latency.

but also extends the applications of the Koopman operator theory to a broader spectrum of research fields.

References

Ahn S, Korattikara A, Liu N, Rajan S, Welling M (2015) Large-scale distributed bayesian matrix factorization using stochastic gradient mcmc. In: KDD '15 Proceedings of the 21rd ACM SIGKDD International Conference on Knowledge Discovery and Data Mining, Sydney, NSW, Australia, pp 9–18

Alotaiby TN, El-Samie FEA, Alshebeili SA, Aljibreen KH, Alkhanen E (2015) Seizure detection with common spatial pattern and support vector machines. In: 2015 International Conference on Information and Communication Technology Research (ICTRC)

Brockett R (1970) Finite Dimensional Linear Systems, Decision and Control, Electronic & Electrical Engineering Research Studies, vol 7. John Wiley & Sons, Inc.

Budišić M, Mohr R, Mezić I (2012) Applied koopmanism. Chaos: An Interdisciplinary Journal of Nonlinear Science 22(4)

Canuta C, Hussaini MY, Quarteroni A, Zang TA (2006) Spectral Methods: Fundamentals in Single Domains. Scientific Computation, Springer-Verlag Berlin Heidelberg

Chou CA, Kampa K, Mehta S, amd W A Chaovalitwongse RT, Grabowski T (2014) Voxel selection framework in multi-voxel pattern analysis of fmri data for prediction of neural response to visual stimuli. IEEE Transactions on Medical Imaging 33(4):925–934

Coutanche MN, Thompson-Schill SL, Schultz RT (2011) Multi-voxel pattern analysis of fmri data predicts clinical symptom severity. Neuroimage 57(1):113–123

Davis JV, Kulis B, Jain P, Sra S, Dhillon IS (2007) Information-theoretic metric learning. In: ICML '07 Proceedings of the 24th international conference on Machine learning, Corvalis, Oregon, USA

Douglas RG (1998) Banach Algebra Techniques in Operator Theory, Graduate Texts in Mathematics, vol 179, 2nd edn. Springer-Verlag New York

Giannakaki G, Sakkalis V, Pediaditis M, Tsiknakis M (2014) Methods for seizure detection and prediction: An overview. Sakkalis V (eds) Modern Electroencephalographic Assessment Techniques Neuromethods 91:131–157

Giannakis D, Slawinska J, Zhao Z (2015) Spatiotemporal feature extraction with data-driven koopman operators. In: Storcheus D, Rostamizadeh A, Kumar S (eds) Proceedings of the 1st International Workshop on Feature Extraction: Modern Questions and Challenges at NIPS 2015, PMLR, Montreal, Canada, Proceedings of Machine Learning Research, vol 44, pp 103–115

Goldberger AL, Amaral LAN, Glass L, Hausdorff JM, Ivanov PC, Mark RG, Mietus JE, Moody GB, Peng CK, Stanley HE (2000) Physiobank, physiotoolkit, and physionet: Components of a new research resource for complex physiologic signals. Circulation 101(3):e215–e220

Gotman J (1982) Automatic recognition of epileptic seizures in the eeg. Electroencephalography and Clinical Neurophysiology 54(5):530 – 540

Hallac D, Vare S, Vare S, Boyd S, Leskovec J (2017) Toeplitz inverse covariance-based clustering of multivariate time series data. In: KDD '17 Proceedings of the 23rd ACM SIGKDD International Conference on Knowledge Discovery and Data Mining, Halifax, NS, Canada, pp 215–223

Haxby J, Gobbini M, Furey M, Ishai A, Schouten J, Pietrini P (2001) Distributed and overlapping representations of faces and objects in ventral temporal cortex. Science 293:2425–2430

Huettel SA, Song AW, McCarthy G (2008) Functional Magnetic Resonance Imaging, 2nd edn. Sinauer Associates

Jain AK, Duin RPW, Mao J (2000) Statistical pattern recognition: A review. IEEE Transactions on Pattern Analysis and Machine Intelligence 22(1):4–37

Khan YU, Rafiuddin N, Farooq O (2012) Automated seizure detection in scalp eeg using multiple wavelet scales. In: 2012 IEEE International Conference on Signal Processing, Computing and Control (ISPCC)

Khanmohammad S, Chou CA (2016) A simple distance based seizure onset detection algorithm using common spatial patterns. In: Brain Informatics and Health, Springer International Publishing, Cham, pp 233–242

Khanmohammad S, Chou CA (2018) Adaptive seizure onset detection framework using a hybrid pca–csp approach. IEEE Journal of Biomedical and Health Informatics 22(1):154–160

Koopman BO (1931) Hamiltonian systems and transformation in hilbert space. In: Proceedings of National Academy of Sciences, vol 17, pp 315–318

Krishnapuram B, Carin L, Hartemink AJ (2004) Joint classifier and feature optimization for comprehensive cancer diagnosis using gene expression data. Journal of Computational Biology 11(2-3):227–242

Lehnertz K, Geier C, Rings T, Stahn K (2017) Capturing time-varying brain dynamics. Nonlinear Biomedical Physics 5(2)

Liu H, Motoda H (1998) Feature Selection for Knowledge Discovery and Data Mining, The Springer International Series in Engineering and Computer Science, vol 454. Springer US

Ma X, Chou CA, Sayama H (2016) Brain response pattern identification of fmri data using a particle swarm optimization-based approach. Brain Informatics 3:181–192

Martino FD, Valent G, Staeren N, Ashburner J, Goeble R (2008) Combining multivariate voxel selection and support vector machines for mapping and classification of fmri spatial patterns. Neuroimage 43(1):44–58

Mezić I (2005) Spectral properties of dynamical systems, model reduction and decompositions. Nonlinear Dynamics 41:309–325

Mezić I (2013) Analysis of fluid flows via spectral properties of the koopman operator. Annual Review of Fluid Mechanics 45(1):357–378

Michel V, Damon C, Thirion B (2008) Mutual information-based feature selection enhances fmri brain activity classification. In: 5th IEEE International Symposium on Biomedical Imaging: From Nano to Macro, 2008. ISBI 2008., pp 592–595

Mitchell TM, Shinkareva SV, Carlson A, Chang KM, Malave VL, Mason RA, Just MA (2008) Predicting human brain activity associated with the meanings of nouns. Science 320(5580):1191–1195

Nasehi S, Pourghassem H (2013) Patient-specific epileptic seizure onset detection algorithm based on spectral features and ipsonn classifier. In: 2013 International Conference on Communication Systems and Network Technologies, pp 186–190

Petersen KE (1983) Ergodic Theory. Cambridge Studies in Advanced Mathematics, Cambridge University Press

Raak F, Susuki Y, Hikihara T (2016) Data-driven partitioning of power networks via koopman mode analysis. IEEE Transactions on Power Systems 31(4):2799 – 2808

de Ridder D, de Ridder J, Reinders MJT (2013) Pattern recognition in bioinformatics. Briefings in Bioinformatics 14(5):633–647

Rowley CW, Mezić I, Bagheri S, Schlatter P, Henningson DS (2009) Spectral analysis of nonlinear flows. Journal of Fluid Mechanics 641:115–127

Saab M, Gotman J (2005) A system to detect the onset of epileptic seizures in scalp eeg. Clinical Neurophysiology 116(2):427–442

Sato I, Nakagawa H (2015) Stochastic divergence minimization for online collapsed variational bayes zero inference of latent dirichlet allocation. In: KDD '15 Proceedings of the 21rd ACM SIGKDD International Conference on Knowledge Discovery and Data Mining, Sydney, NSW, Australia, pp 1035–1044

Schomer DL, da Silva FL (2010) Niedermeyer's Electroencephalography: Basic Principles, Clinical Applications, and Related Fields, 6th edn. Lippincott Williams and Wilkins

Shamir L, Delaney JD, Orlov N, Eckley DM, Goldberg IG (2010) Pattern recognition software and techniques for biological image analysis. PLoS Computational Biology 6(11):e1000974

Shoeb A (2009) Application of machine learning to epileptic seizure onset detection and treatment

Smith SM (2004) Overview of fmri analysis. Br J Radiol 77(Spec No. 2):167–175

Susuki Y, Mezić I, Hikihara T (2011) Coherent swing instability of power grids. Journal of Nonlinear Science 21(3):403–439

Susuki Y, Mezić I, Raak F, Hikihara T (2016) Applied koopman operator theory for power systems technology. Nonlinear Theory and Its Applications pp 430–459

Walters P (1982) An Introduction to Ergodic Theory, Graduate Texts in Mathematics, vol 79, 1st edn. Springer-Verlag New York

Wilkinson DJ (2006) Bayesian methods in bioinformatics and computational systems biology. Briefings in Bioinformatics 8(2):109–116

Wilson S, Scheuer M, Emerson R (2004) Seizure detection: Evaluation of the reveal algorithm. Clinical Neurophysiology 115(10):2280–2291

Wilson SB (2005) A neural network method for automatic and incremental learning applied to patient-dependent seizure detection. Clinical Neurophysiology 116(8):1785–1795

Wilson SB (2006) Algorithm architectures for patient dependent seizure detection. Clinical Neurophysiology 117(6)

Zhao Y, Ahmed B, Thesen T, Blackmon KE, Dy JG, Brodley CE (2016) A non-parametric approach to detect epileptogenic lesions using restricted boltzmann machines. In: KDD '16 Proceedings of the 22rd ACM SIGKDD International Conference on Knowledge Discovery and Data Mining, San Francisco, CA, USA, pp 373–382